Preparation of Fe-Co-based bulk amorphous alloy from high purity and industrial raw materials

S. Lesz*

Division of Nanocrystalline and Functional Materials and Sustainable Pro-ecological Technologies,
Institute of Engineering Materials and Biomaterials, Silesian University of Technology,
ul. Konarskiego 18a, 44-100 Gliwice, Poland
* Corresponding author: E-mail address: sabina.lesz@polsl.pl

ABSTRACT

Purpose: The main aim of the paper was preparation of Fe-Co-based bulk amorphous alloy from high purity and industrial raw materials by an ejection copper mold casting method.

Design/methodology/approach: The following experimental techniques were used: differential thermal analysis (DTA), scanning electron microscopy (SEM), light microscopy (LM), X-ray diffraction (XRD) method, Vickers microhardness.

Findings: In this work comparison of structure and properties of Fe-Co-based bulk metallic glasses (BMGs) prepared from both high purity and industrial materials were presented.

Research limitations/implications: Obtained structures are dependent on cooling rate and glass forming ability of the alloy prepared from high purity materials and from industrial (ferroalloys) materials.

Practical implications: The successful preparation of the Fe-Co-based bulk metallic glasses from industrial raw materials will benefit cost-effective development of functional materials.

Originality/value: In this work, an attempt has been made to prepare the Fe-Co-based BMGs more economically by means of replacement of high purity materials with industrial (ferroalloys) materials.

Keywords: Amorphous materials; High purity and industrial materials; XRD, SEM and LM method; Microhardness

Reference to this paper should be given in the following way:

S. Lesz, Preparation of Fe-Co-based bulk amorphous alloy from high purity and industrial raw materials, Archives of Materials Science and Engineering 48/2 (2011) 77-88.

MATERIALS

1. Introduction

In the last decades, great effort have been devoted to process Fe-based bulk metallic glasses (BMG) because of their fundamental scientific interest and promising potential for industrial applications. BMGs were obtained at the relatively low cooling rate of less than 100 K/s from liquid state by stabilization of the supercooled liquid against crystallization in various multi-component metallic alloys [1-9]. The advent of thicker glassy ferromagnetic foils will be of tremendous benefit [10].

Among the large number of BMGs, Fe-based BMGs are the most attractive due to many superior properties such as high mechanical strength, good deformability in the supercooled liquid region, strong corrosion resistance, low hysteresis losses and low current losses under cyclic magnetic excitation, as well as abundant natural resources and relatively low material cost [1-18].

The high purity of raw materials and the strict processing cause a high cost for production of BMGs, which is one of the key problems restricting their the widely industrial applications. Thus preparing BMG from industrial raw materials is desirable.

Some industrial ferroalloys having high carbon and high silicon contents exhibited high glass forming ability (GFA) [11]. On the other hand the presence of even traces of oxygen and other impurities would induce the heterogeneous nucleation and cause difficulties for fully amorphous structure and pose a problem with obtaining eutectic composition [10,12]. Therefore the solution of these limitations is part of interesting and innovative research work.

Generally, bulk ferromagnetic glasses can be prepared from the melts by techniques: copper casting and flux-melting +water-quenching. The maximum diameter of Fe-base bulk amorphous rods that can be prepared by a copper mould casting method has been reported to be 12 mm for the $Fe_{48}Cr_{15}Mo_{14}Er_2C_{15}B_6$ [13], $(Fe_{44.3}Cr_{10}Mo_{13.8}Mn_{11.2}C_{15.8}B_{5.9})_{98.5}Y_{1.5}$[14], $Fe_{44.3}Cr_5Co_5Mo_{12.8}Mn_{11.2}C_{15.8}B_{5.9})_{98.5}Y_{1.5}$ [14]. High GFA of these alloys is attributed to the addition of optimum amounts of noble elements such as Er and Y [11]. For obtaining samples with larger sizes and securing high GFA, besides using high purity raw materials, an inert atmosphere during materials processing and flux treatment methods were also applied to the Fe-based alloys [10-12,15,16].

The paper reports the preparation of $Fe_{36}Co_{36}B_{19}Si_5Nb_4$ BMG from the high purity and industrial (ferroalloys) raw materials by an ejection copper mold casting method.

2. Experimental procedure

Investigations were carried out on bulk metallic glass in a form of rods with compositions of $Fe_{36}Co_{36}B_{19}Si_5Nb_4$.

The Fe-based master alloy ingots with above compositions were prepared by arc melting of raw materials under argon atmosphere.

The raw materials designed for produce BMG from the high purity were pure Fe, Co, Nb metals and non-metallic elements: Si, B.

The raw materials used in this experiment for produce BMG from the industrial materials were pure Fe, Co metals and ferroalloy: Fe-B, Fe-Si, Fe-Nb which contains Fe and 14.5 mass% of B, 57.2 mass% of Si, 68.5 mass% of Nb, respectively and other constitutes, such as aluminum, carbon, sulfur, phosphorus and their oxides in remainder. The content of boron in the cast alloy was adjusted by adding the Fe-B alloy, which is much cheaper than pure boron.

The master alloy was melted in a quartz crucible using an induction coil. Each ingot was re-melted several times to ensure the chemical homogeneity of the samples, and then was eject into a water-cooled copper split mould with square form under argon atmosphere. The investigated materials were cast as rods shaped with square section with side of 1.5 and 2.5 mm.

From a few rods produced from industrial materials the rods with square section with side of 1.5 mm (cast 1, cast 2) and 2.5 mm (cast 1) was selected to further investigations due to the same phase composition.

Thermal properties (liquidus -T_l , solidus - T_s , eutectic - T_e temperatures) of the pre-alloyed ingots upon heating and cooling were analyzed by a NETZSCH model DSC 404 C Pegasus under a continuous argon flow, at the heating and cooling rate of 0.33 K/s. The onset and end of the peak was determine using tangent method [19].

The microstructure of the rods was examined by X-ray diffraction (XRD) and light microscopy method (LM).

The X-ray method has been performed by the use of diffractometer XRD 7, Seifert-FPM firm, with filtered Co-Kα radiation. X-ray diffraction patterns of the were performed from surface of rods with square section 1.5 and 2.5 mm.

In order to conduct structural study, the light microscope LEICA MEF 4A in the range of 100× to 1000× magnitude was used. In addition, of the $Fe_{36}Co_{36}B_{19}Si_5Nb_4$ rods with square section with side of 1.5 and 2.5 mm, prepared from industrial raw materials on the etched cross-sectional surface was examined by means of the scanning electron microscope (SEM) SUPRA 25, ZEISS. The chemical composition (without boron) of micro-areas (phases) in different zones of rods was fixed by means of the point - by - point method, using a scattered X - radiation detector (EDS) produced by EDAX, which is a part of scanning electron microscope equipment.

Microhardness was measured with a use of the Vickers hardness tester FUTURE-TECH FM-700 under the load of 0.49 N (50 G) [20].

3. Results and discussion

The base master $Fe_{36}Co_{36}B_{19}Si_5Nb_4$ alloy produced from the high purity elements and produced from the industrial materials differ in thermal stability (T_e and T_l).

The DTA curve of the base master alloy produced from the high purity elements under the heating shows two endothermic peaks (Fig. 1). The first peak for base alloy begins near the eutectic (melting) point - T_e =1194 K. The maximum signal of the second peak is separate and occurs in temperature range from 1329 to 1386 K. This signal is associated with the liquidus temperature T_l [19]. Such DTA trace under the heating is connected with transit of hardsoluble crystalline phases into the liquid state.

Only one major peak is observed in Fig. 1 - DTA curves of the base master alloy produced from the high purity elements under the cooling. This peak is undoubtedly the crystallization temperature and the onset of the peak occurs at temperature1268 K. This peak is the eutectic transformation temperature and indicated that chemical composition of investigated alloy was chosen correct. From DTA analysis the onset of solidification occurs at 1268 K and end at 1213 K. The onset of solidification corresponds to the eutectic temperature T_e (Fig. 1) [19].

The DTA traces of the base master alloy produced from the high purity elements (Fig. 1) is differ from the base master alloy produced from the industrial materials (Fig. 2).

A few peaks are observed on the DTA curves of the $Fe_{36}Co_{36}B_{19}Si_5Nb_4$ produced from the industrial materials under the heating and cooling (Fig. 2). The DTA trace of the base master alloy ingot under the heating exhibit two exothermic

reactions. The first peak begins at the temperature 1312 K and is associated with melting process. The end of the second peak can be determined to be 1430 K and corresponds to the liquidus temperature - T_l.
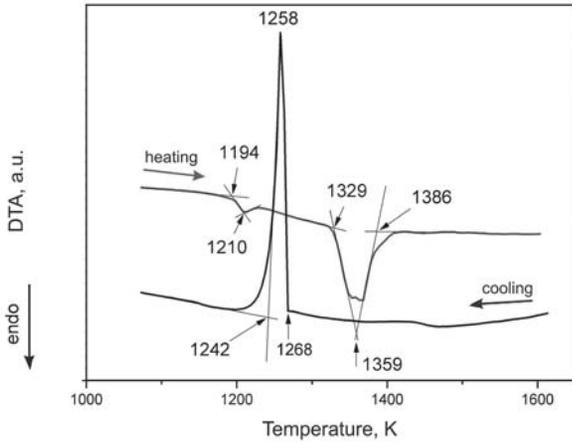
Fig. 1. Differential thermal analysis (DTA) curves of the base master alloy ingot for produce BMG from the high purity materials under the heating/cooling rate of 0.33 K/s
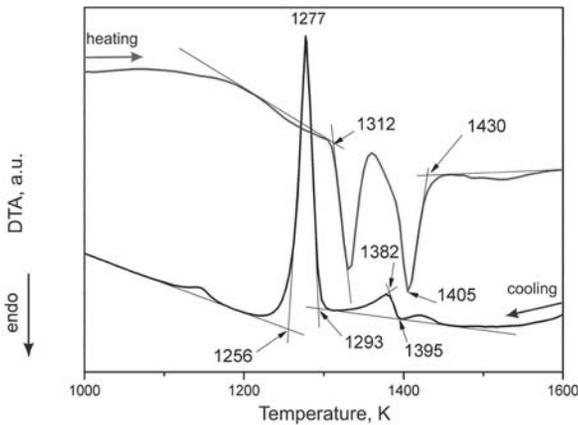
Fig. 2. Differential thermal analysis (DTA) curves of the base master alloy ingot for produce BMG from the industrial materials under the heating/cooling rate of 033 K/s

On the DTA curve of the $Fe_{36}Co_{36}B_{19}Si_5Nb_4$ alloy produced from the industrial materials under the cooling two peaks are clearly shown (Fig. 2). The first peak corresponds to the liquidus temperature - T_l (1395 K) however the onset of the second peak occurs at temperature 1293 K. This peak is the eutectic transformation temperature - T_e.

Two melting events demonstrate that the base alloy prepared from industrial materials is different from the eutectic composition. This result indicates that during casting into fully amorphous structure of the $Fe_{36}Co_{36}B_{19}Si_5Nb_4$ alloy using industrial raw materials technological difficulties may occur.
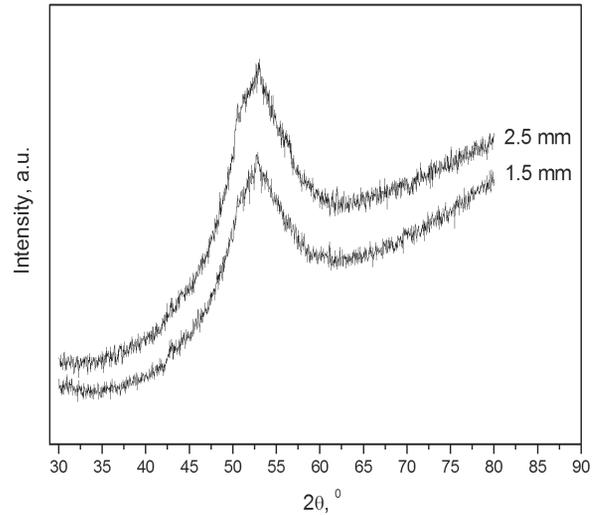
Fig. 3. X-ray diffraction pattern taken from the surface of the $Fe_{36}Co_{36}B_{19}Si_5Nb_4$ rods with square section with side of 1.5 mm and 2.5 mm prepared from the high purity raw materials
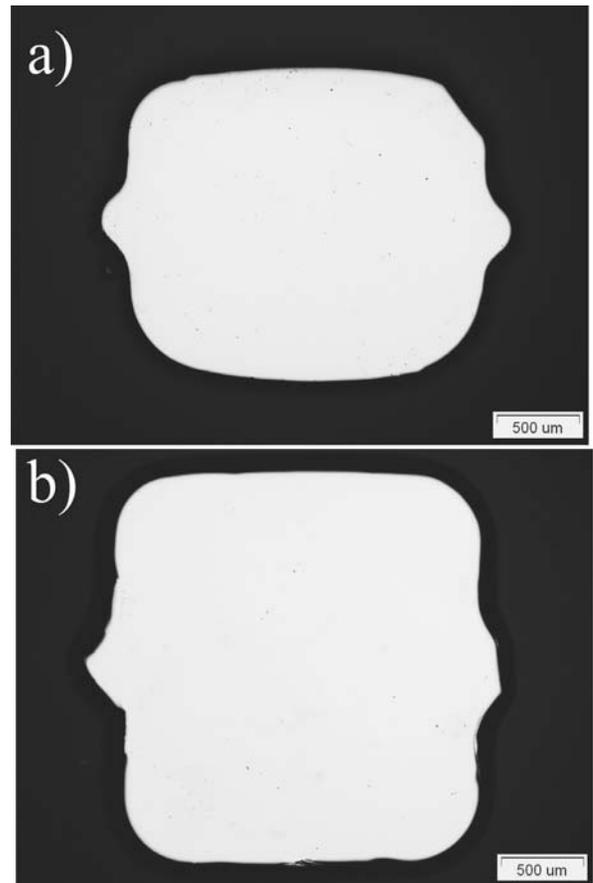
Fig. 4. Optical micrographs of the transverse cross sections after etching of the $Fe_{36}Co_{36}B_{19}Si_5Nb_4$ rods with square section with side of 1.5 (a) and 2.5 mm (b) prepared from the high purity raw materials
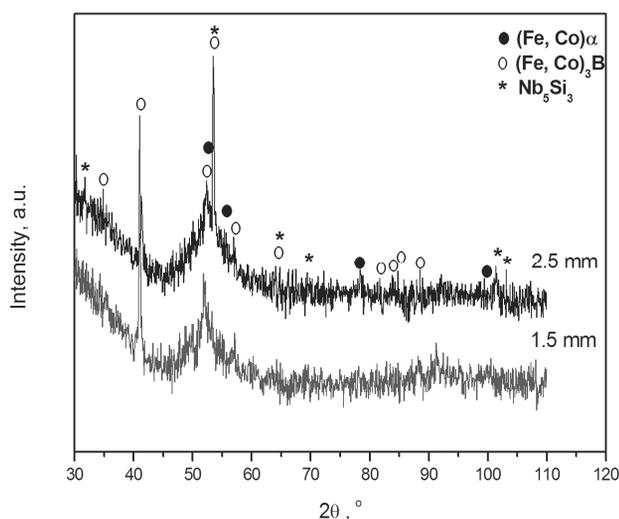
Fig. 5. X-ray diffraction pattern taken from the surface of the $Fe_{36}Co_{36}B_{19}Si_5Nb_4$ rods with square section with side of 1.5 mm and 2.5 mm (cast 1) prepared from the industrial raw materials

The structure of the surface of rods produced from the high purity materials is amorphous what was proved in the X-ray diffraction patterns (Fig. 3). The diffraction patterns consist of only broad peaks for these rods and no detectable crystalline peaks are seen, indicating the formation of amorphous single phase only. Occurrence of amorphous single phase was confirmed in the light microscopy (LM) results (Fig. 4). The transverse cross-sectional structure of the $Fe_{36}Co_{36}B_{19}Si_5Nb_4$ rods with square section with side of 1.5 mm and 2.5 mm prepared from the

high purity raw materials with good metallic luster was found to be very bright and glass-like (Fig. 4).

The results of X-ray diffraction method of selected rods with square section with side of 1.5 mm and 2.5 mm (cast 1) produced from industrial materials indicates that their phase composition is the same (Fig. 5). In the XRD patterns a few of Bragg's peaks superimposed on the diffused diffraction maxima, which means that the rods contain crystalline phases. The crystalline phases are identified as $(Fe, Co)\alpha$, $(Fe, Co)_3B$ and Nb_5Si_3.
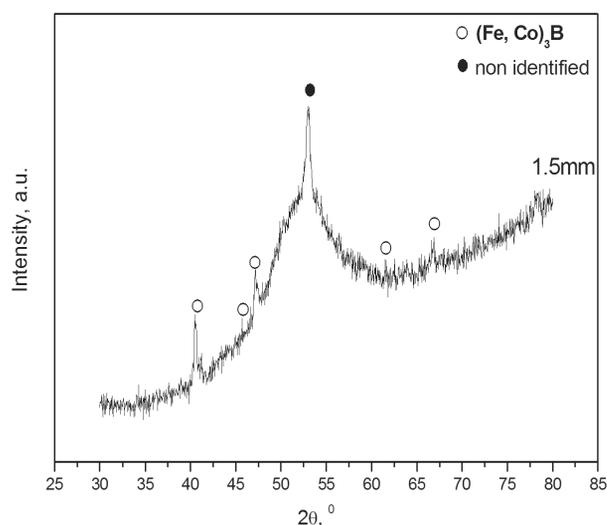
Fig. 6. X-ray diffraction pattern taken from the surface of the $Fe_{36}Co_{36}B_{19}Si_5Nb_4$ rod with square section with side of 1.5 mm (cast 2) prepared from the industrial raw materials

Table 1.
The chemical composition (results of EDS analysis) and microhardness of phases existed in the structure of $Fe_{36}Co_{36}B_{19}Si_5Nb_4$ rods with square section with side of 1.5 mm and 2.5 mm (cast 1) prepared from the industrial raw materials

Colour of phases after etched	Side of square section of rod	The chemical composition, %at.				Figure	Microhardness, HV
		Fe	Co	Si	Nb		
light	1.5	44.26	42.40	7.01	6.33	Fig. 9	1284
light	1.5	44.26	42.40	7.01	6.33	Fig. 12b	-1573
light	2.5	44.40	43.85	6.13	5.62	Fig. 10	1330
light	2.5	41.76	44.26	7.75	6.23	Fig. 15a	-1542
average		43.67±1.30	43.23±1.00	6.98±0.70	6.13±0.34		
dark	1.5	39.49	40.17	9.35	11.00	Fig. 12c	1780-1923(B-zone)
dark	2.5	41.50	43.41	8.68	6.41	Fig. 15c	1735-1974(B-zone)
average		40.5±1.42	41.79±2.3	9.02±0.47	8.71±3.25		
black	1.5	39.28	40.15	11.60	8.97	Fig. 13a	2142
black	1.5	42.72	40.29	9.41	7.58	Fig. 13b	-2332 (C-zone)
black	1.5	42.14	40.05	9.64	8.17	Fig. 13c	
black	2.5	41.15	42.62	8.08	8.15	Fig. 16a	1882
black	2.5	42.11	44.83	6.76	6.30	Fig. 16b	-2236(C-zone)
black	2.5	39.13	45.03	8.49	7.35	Fig. 16c	
average		41.09±1.41	42.16±2.14	9.00±1.50	7.75±0.83		
light with visible	1.5	20.36	20.16	7.02	52.46	Fig. 12a	1341-1537 (C-zone)
grain boundary	2.5	16.32	20.38	7.59	55.72	Fig. 15b	1311-1467 (C-zone)
average		18.34±2.02	20.27±0.11	7.31±0.29	54.09±1.63		
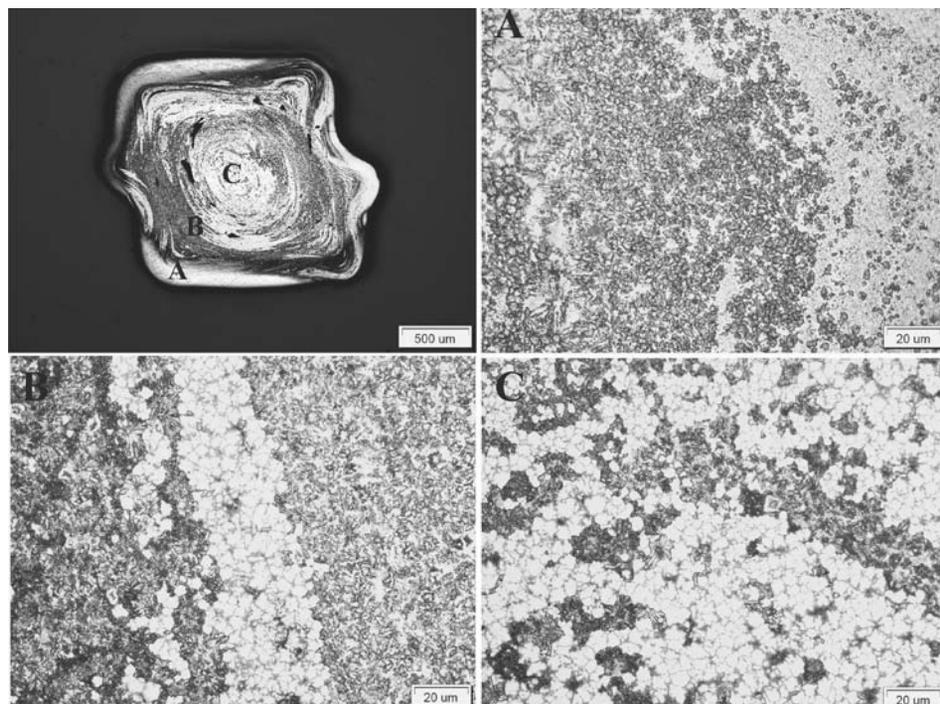
Fig. 7. Optical micrographs of the transverse cross sections after etching of the $Fe_{36}Co_{36}B_{19}Si_5Nb_4$ rods with square section with side of 1.5 mm prepared from the industrial raw materials; A- zone having contact with the copper mould during cooling, B- zone - region between surface and core of rod, C- zone - core of rod
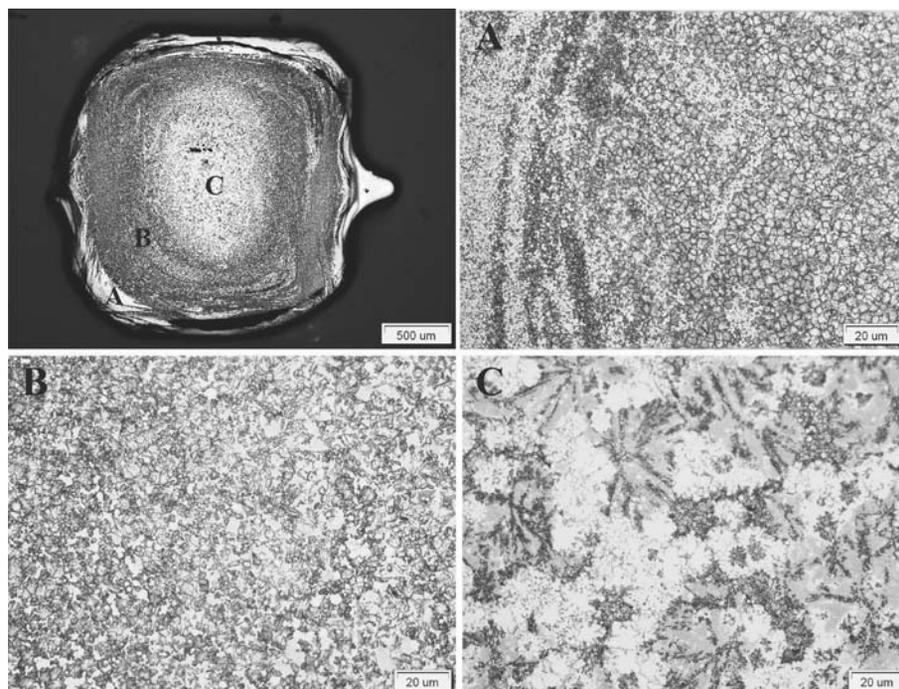
Fig. 8. Optical micrographs of the transverse cross sections after etching of the $Fe_{36}Co_{36}B_{19}Si_5Nb_4$ rods with square section with side of 2.5 mm prepared from the industrial raw materials; A- zone having contact with the copper mould during cooling, B- zone - region between surface and core of rod, C- zone - core of rod
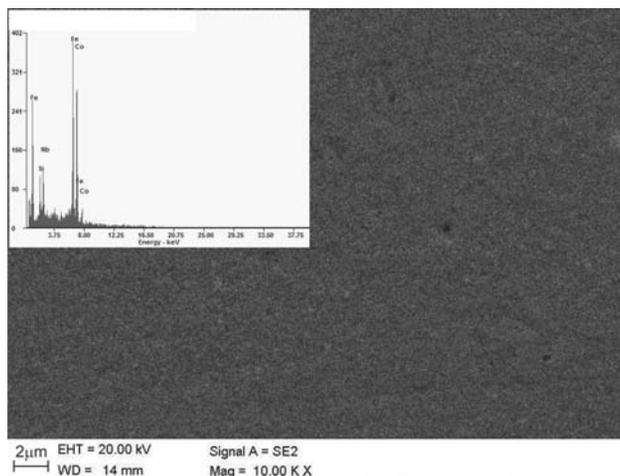
Fig. 9. SEM backscattered electron micrograph of the Fe$_{36}$Co$_{36}$B$_{19}$Si$_5$Nb$_4$ rods with square section with side of 1.5 mm prepared from the high purity raw materials on the etched cross-section surface: the image no hint for any visible crystallization phase - amorphous structure
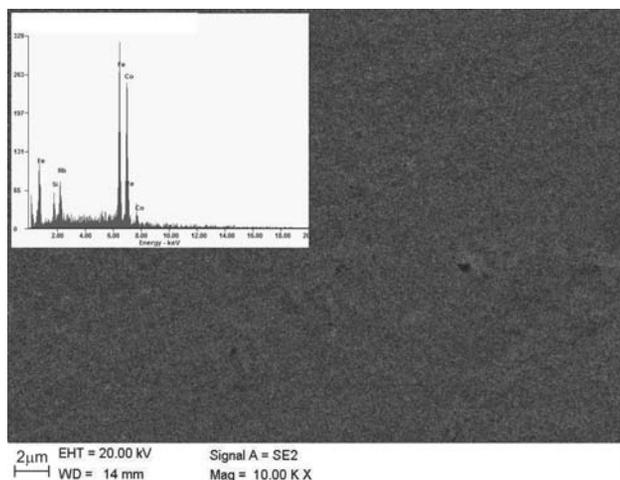
Fig. 10. SEM backscattered electron micrograph of the Fe$_{36}$Co$_{36}$B$_{19}$Si$_5$Nb$_4$ rods with square section with side of 2.5 mm prepared from the high purity raw materials on the etched cross-section surface: the image no hint for any visible crystallization phase - amorphous structure

The phase composition of surface of rod with square section with side of 1.5 mm (cast 2) (Fig. 6) produced from industrial materials is different from the phase composition of above-mentioned rods (cast 1) (Fig. 5). The diffraction pattern taken from the surface of this rod (cast 2) exhibits broad halo peak typical for amorphous phase and a set of several weak crystalline peaks (Fig. 6). These diffraction peaks correspond to the crystalline (Fe,Co)$_3$B and an non identified phase. These results indicating that in these rods a mixed structure of amorphous matrix together

with crystalline phases was formed. The possible reason is that ferroalloys addition can suppress the precipitation of the (Fe,Co)$_3$B, Nb$_5$Si$_3$ and (Fe,Co)α, crystalline compounds during the cast process. According to Y. Hu [12] significant is establish a proper metalloids addition which can improve GFA, but too much addition leads to the precipitation of crystalline phase.

The positive effects of multi-metalloids addition on GFA can be understood from structural viewpoint. There is more than one kind of metalloid with different atomic size in the alloy, it is expected to obtain a larger dense random packing in the supercooled liquid. Existence not only kind of metalloid in alloy makes the redistribution of atoms on a large range scale and difficult for cooling process. On the other hand, the mobility of atoms in cooling process is a key for the nucleation and growth of a crystalline phase [12].

The Fe$_{36}$Co$_{36}$B$_{19}$Si$_5$Nb$_4$ rods with square section with side of 1.5 mm and 2.5 mm (cast 1) produced from industrial materials have different structure on surface, in core and in transition zone. After etched the different microstructure zones were exposed (A, B, C in Figs. 7, 8). On the sample's edge, zone having contact with the copper mould during cooling (A- zone) occurs homogenous light-etched zone indicating the existence of small amount of amorphous phase (Figs. 7, 8) [21]. Results of SEM confirm existence of the amorphous phase beside the crystalline phases (Figs. 9-16). The existence of amorphous phase in this zone is caused by high speed heat abstraction. Visible dark-etched crystalline phase with 1-4 μm grain size in this zone was observed (Figs. 7, 8).

In B - zone, region between surface and core of the rod, both light-etched crystalline phase with 4-8 μm grain size, dark-etched and black-etched zones (Figs. 7, 8) were observed. However C-zone, core of the rod, had the similar structural composition. Additionally in B and C zone presence of acicular eutectic rosette shaped (Figs. 7, 8) as well light twinned grains round which occurs black zones (Figs. 11-13) were observed.
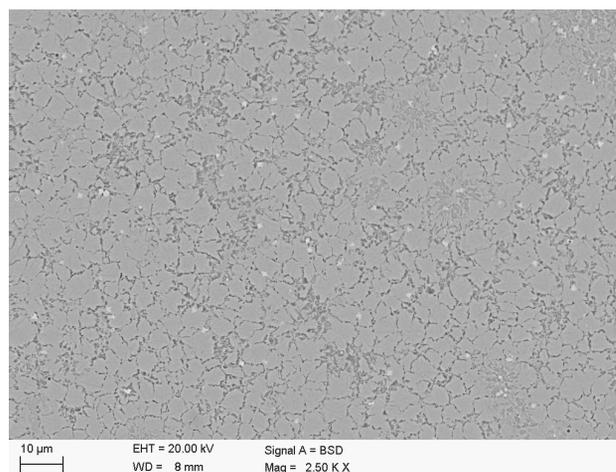
Fig. 11. SEM backscattered electron micrograph of the Fe$_{36}$Co$_{36}$B$_{19}$Si$_5$Nb$_4$ rods with square section with side of 1.5 mm prepared from the industrial raw materials on the etched cross-section surface: the amorphous phase, black-etched crystalline phase and sphere-form precipitates
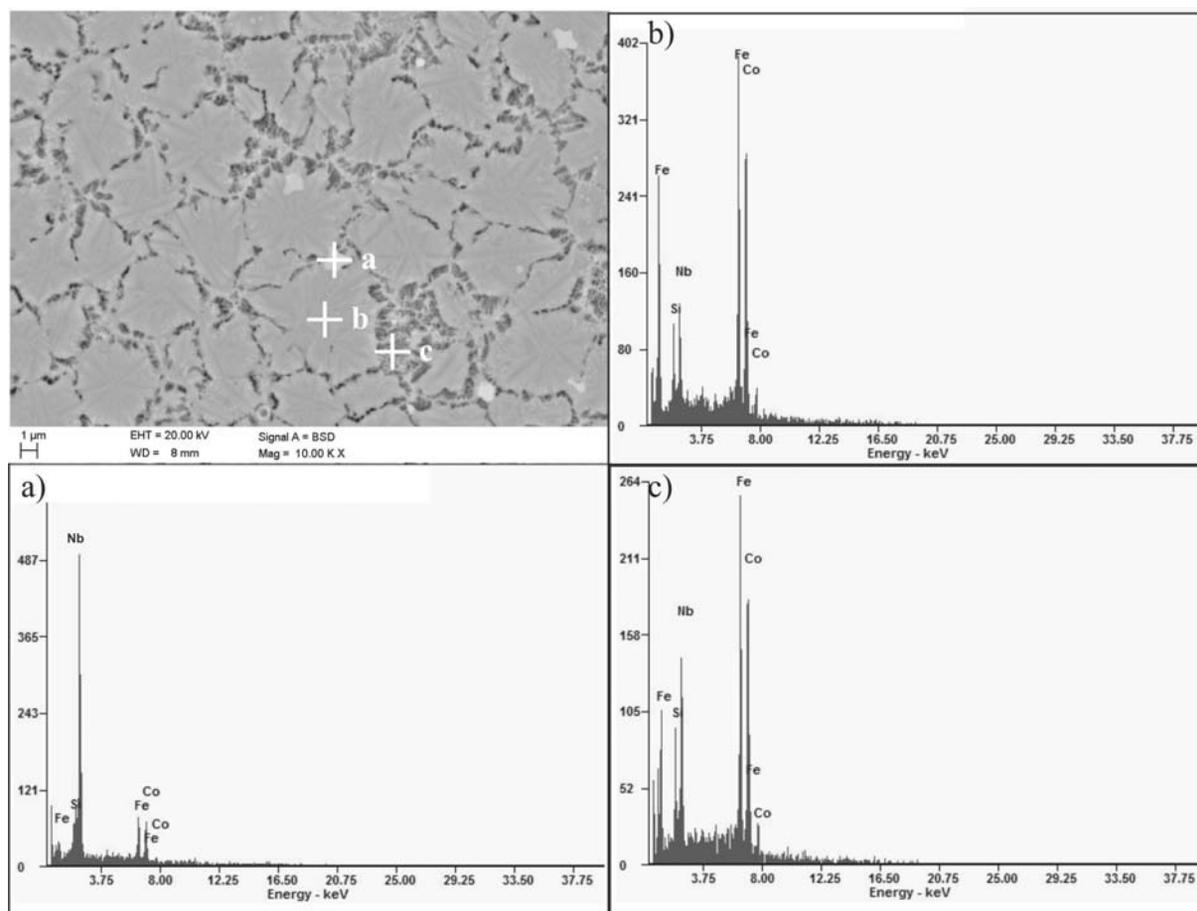
Fig. 12. SEM backscattered electron micrograph of $Fe_{36}Co_{36}B_{19}Si_5Nb_4$ rod with square section with side of 1.5 mm (cast 1) prepared from the industrial raw materials on the etched cross-section surface: a, b, c - the places of EDS analysis with results

The light-etched zone amorphous phase presents in the surface of rods with square section with side of 1.5 and 2.5 mm produced from industrial materials shows existence of the following elements: Fe = 43.67±1.30, Co = 43.23±1.00 Si = 6.98±0.70, Nb = 6.13±0.34 at.% (Figs. 9, 10, 12b, 15a, Table 1).

The obtained results of microanalysis of chemical composition examined by scanning electron microscope (SEM), shows conformity with assumption of the chemical composition. The dark-etched phases shows existence of Fe = 40.5±1.42, Co = 41.79±2.30, Si = 9.02±0.47 and Nb = 8.71±3.25%at. (Figs. 12c, 15c, Table 1). In these phases insignificant increase of Si and Nb concentration occurs. However the black-etched phases shows existence of Fe = 41.09±1.41, Co = 42.16±2.14, Si = 9.00±1.50 and Nb = 7.75±0.83%at. (Figs. 13, 16, Table 1). In the core of the rod white sphere-form precipitations (Figs. 11, 12, 14, 15) are observed, which chemical composition is the following: Fe = 18.34±2.02, Co = 20.27±0.11, Si = 7.31±0.29 and Nb = 54.09±1.63%at (Figs. 12a, 15b, Table 1). The increase of Nb concentration (54.09±1.63% at.) shows that it is probably Nb_5Si_3 phase, which was identified by XRD method (Fig. 5).

It was found from the transverse cross-sectional structure of the rod with square section with side of 1.5 mm (cast 2) produced

from industrial materials after etching studied in light microscope (LM) was smooth and has metallic luster (Fig. 17). After etched the significant homogenous light-etched zone was exposed, which indicated that the existence of amorphous phase in the main. Additionally, dark-etched crystalline phases with eutectic form, were observed (Fig. 17).

Microhardness varies between 1100-1133 HV on the surface of the rod with square section with side of 1.5 mm produced from high purity raw materials. Similarly, value of microhardness keep at a constant level to distance from the sample's edge about 0.4 mm. However microhardness increases to 1160 HV in the core of the rod (Fig. 18). These changes of microhardness are probably connected with structure relaxation. In the core of the rod, where cooling rate of rods during casting is lower, the structure is more relaxed. Thus increase of microhardness is due to decay of free volume content (microvoids) proceed at first stage of relaxation process.

Microhardness on the surface of rod with square section with side of 2.5 mm produced from high purity raw materials to distance from the sample's edge about 1.0 mm is constant and equal 1180 HV, which corresponds to strongly relaxed amorphous structure. However microhardness in the core of the rod is equal to 1230 HV (Fig. 18).
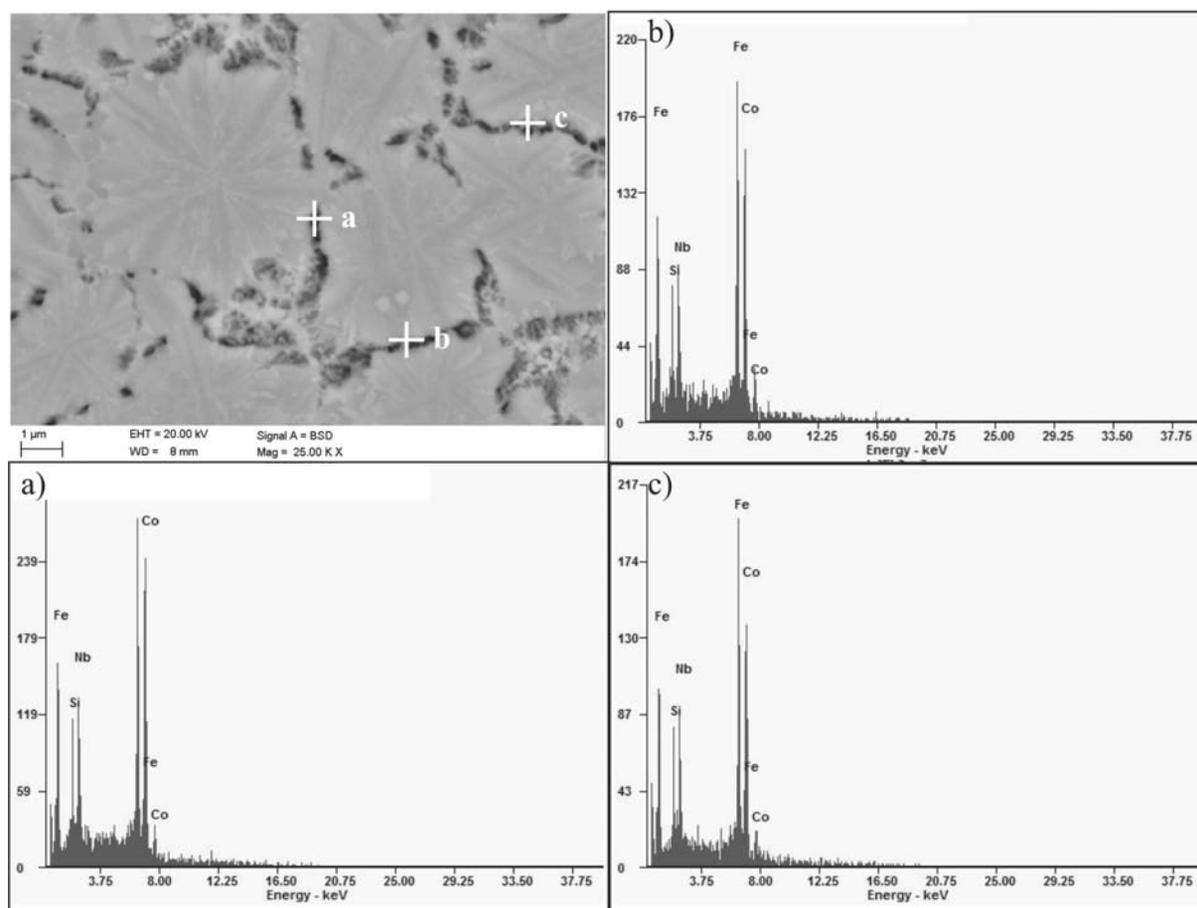
Fig. 13. SEM backscattered electron micrograph of $Fe_{36}Co_{36}B_{19}Si_5Nb_4$ rod with square section with side of 1.5 mm (cast 1) prepared from the industrial raw materials on the etched cross-section surface: a, b, c - the places of EDS analysis with results

Significant differences of microhardness on the cross section of the $Fe_{36}Co_{36}B_{19}Si_5Nb_4$ rods with square section with side of 1.5 and 2.5 mm prepared from the industrial raw materials have been stated. Value of microhardness from 1341 to 2332 HV and from 1312 to 1975 HV have been observed on rod with square section with side of 1.5 and 2.5 mm (cast 1), respectively. In the structure, on the cross section samples, phases with different values of microhardness are observed: homogeneous light-etched phase, the light-etched phase with visible grain boundaries and dark-etched phase (Table 1). In A-zone of the rod with square section with side of 1.5 mm (cast 1), the light-etched phase have value of microhardness from 1284-1573 HV (Table 1). In B and C zone the light-etched phase with visible grain boundaries has value of microhardness from 1501-1573 HV and from 1341-1537 HV, respectively (Table 1). The microhardness of dark-etched phase have value from 1780-1923 HV and black-etched phase: from 2142-2332 HV in B and C zone, respectively (Table 1).

In A - zone of the rod with square section with side of 2.5 mm (cast 1), the microhardness of light-etched phase with visible grain boundaries have value of 1692 HV (Table 1). In B and C zones these light-etched phase have value of microhardness from 1467-1574 HV and from 1311-1467 HV, respectively (Table 1). Microhardness of dark-etched phase have value from 1735-1974 HV in B zone
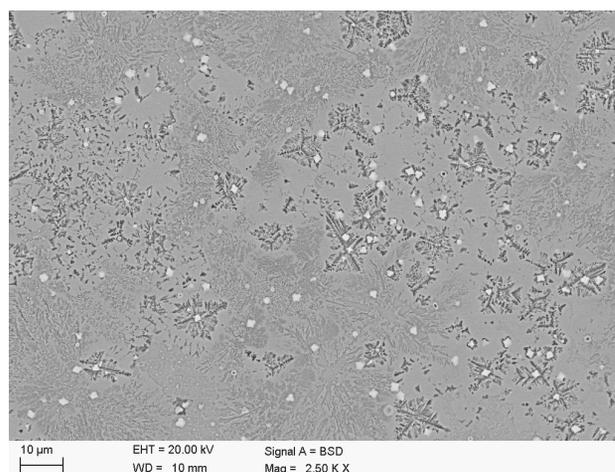
Fig. 14. SEM backscattered electron micrograph of the $Fe_{36}Co_{36}B_{19}Si_5Nb_4$ rods with square section with side of 2.5 mm prepared from the industrial raw materials on the etched cross-section surface: the amorphous phase, black-etched crystalline phase and sphere-form precipitates
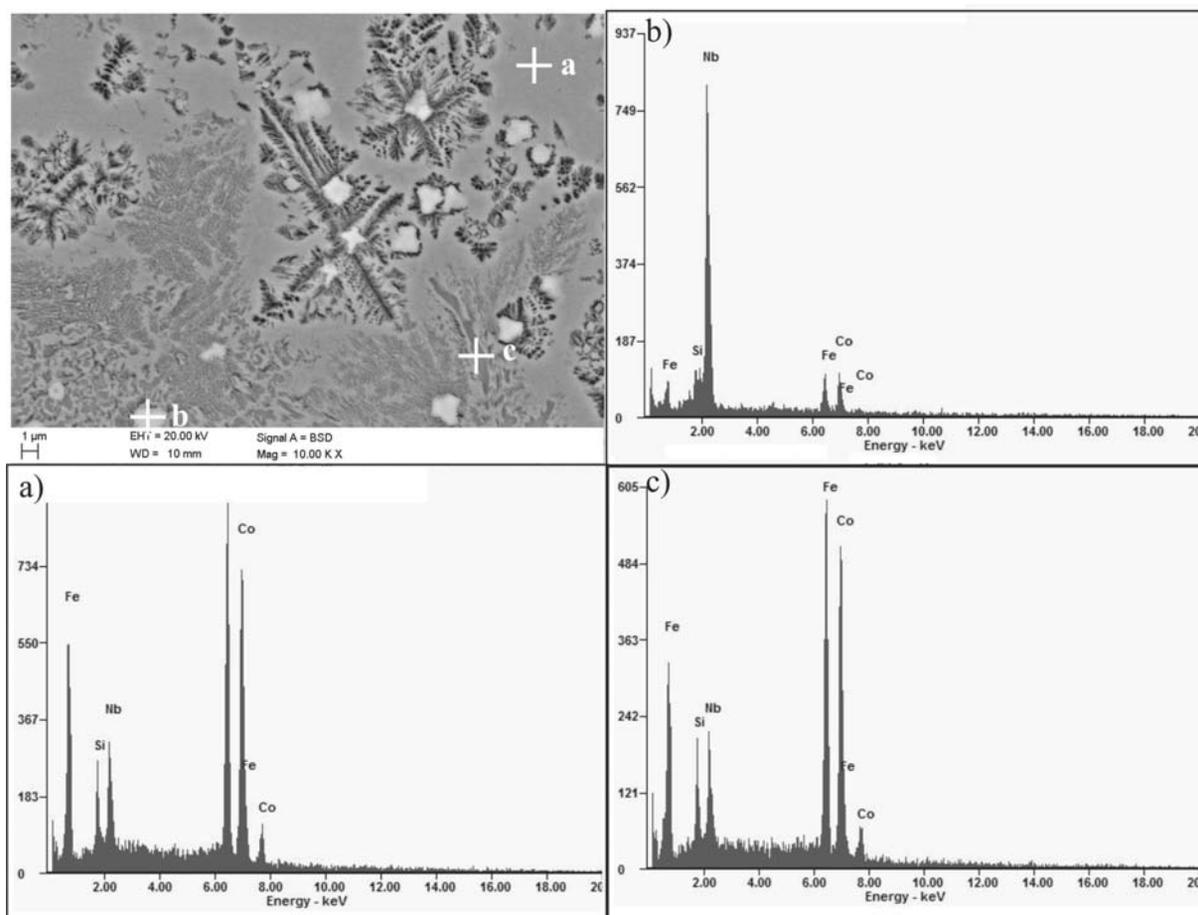
Fig. 15. SEM backscattered electron micrograph of $Fe_{36}Co_{36}B_{19}Si_5Nb_4$ rod with square section with side of 2.5 mm (cast 1) prepared from the industrial raw materials on the etched cross-section surface: a, b, c - the places of EDS analysis with results

(Table 1). Result from microhardness test that black-etched phase have maximum value of microhardness (1882-2236 HV). The light-etched zone amorphous phase occurs in every zones have value of microhardness from 1330-1542 HV (Table 1).

The obtained results show that the microhardness of amorphous phase is far lower (1330-1542 HV) than that of crystalline phase (1882-2236 HV), which is different from the general idea that the microhardness of metallic glasses is higher than that of crystalline alloys. The same trend was observed in $(Fe_{40}Ni_{40}P_{14}B_6)_{96}Ga_4$ alloy [10].

A small difference of the microhardness on the cross section of the $Fe_{36}Co_{36}B_{19}Si_5Nb_4$ rod with square section with side of 1.5 mm (cast 2) produced from industrial materials, consisting of large amount of amorphous phase in structure (confirmed in XRD and LM results) have been observed. The microhardness was in the range from 1204-1257 HV. The microhardness of dark-etched phases occur in the core of the rod has value from 1501-1780 HV (additionally measurements, non marked in Fig. 19).

The obtained results proved that formation of homogeneous amorphous single phase in the structure of rods prepared from industrial raw materials is difficult. Due to the existence of crystalline phases in the structure of rods prepared from industrial raw materials properties of the alloy are different from rods prepared from high purity raw materials. Exception is the $Fe_{36}Co_{36}B_{19}Si_5Nb_4$ rod with square section with side of 1.5 mm (cast 2) produced from industrial materials, consisting of large amount of amorphous phase in structure. It has been demonstrated that the bulk amorphous alloy can be prepared from industrial raw materials

4. Conclusions

The obtained results are summarized as follows:
- Fe-base alloy with compositions of $Fe_{36}Co_{36}B_{19}Si_5Nb_4$ can be produced by copper mould casting using the low cost industrial raw materials (ferroalloy Fe-B).
- The rods with square section with side of 1.5 mm and 2.5 mm (cast 1) produced from industrial materials are amorphous matrix composites consisting of amorphous matrix and crystalline phases. The structure of the rod with square section with side of 1.5 mm (cast 2) prepared by a copper mold casting method without any flux treatment consists of large amount of amorphous phase.
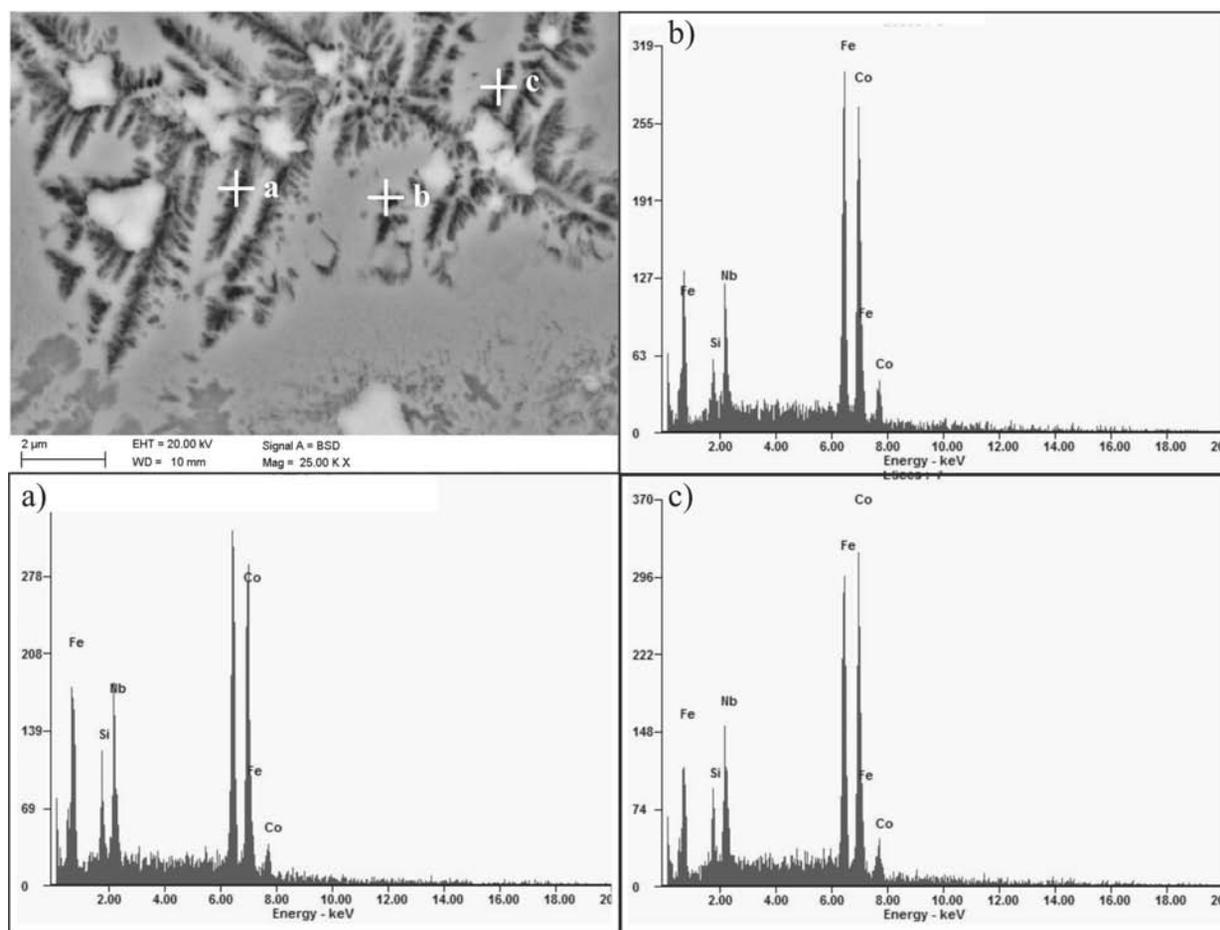
Fig. 16. SEM backscattered electron micrograph of $Fe_{36}Co_{36}B_{19}Si_5Nb_4$ rod with square section with side of 2.5 mm (cast 1) prepared from the industrial raw materials on the etched cross-section surface: a, b, c - the places of EDS analysis with results
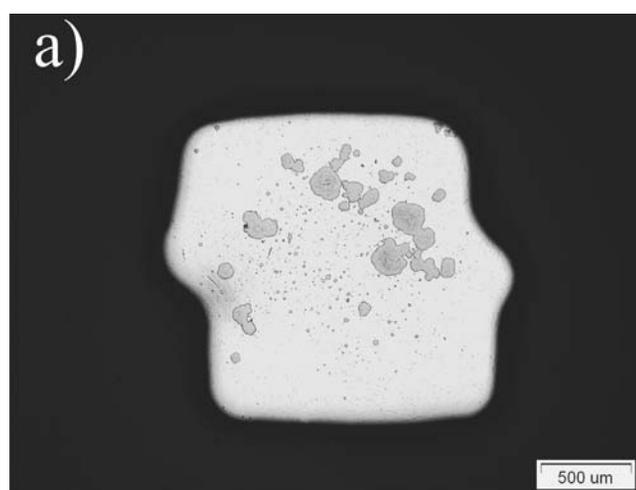
Fig. 17. Optical micrographs of the transverse cross sections after etching of the $Fe_{36}Co_{36}B_{19}Si_5Nb_4$ rods with square section with side of 1.5 mm prepared from the industrial raw materials
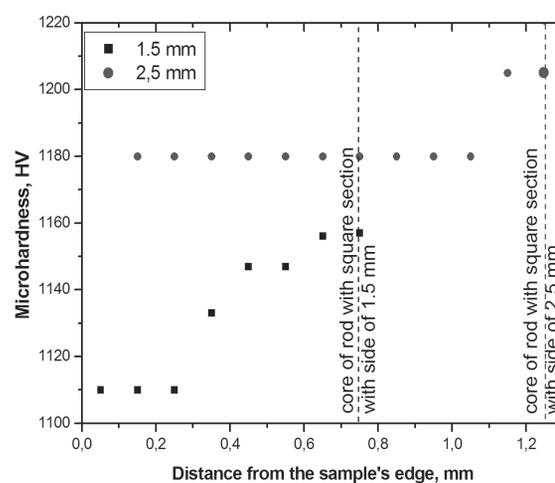
Fig. 18. Results of the microhardness experiments of $Fe_{36}Co_{36}B_{19}Si_5Nb_4$ rods with square section with side of 1.5 mm and 2.5 mm prepared from the high purity raw materials
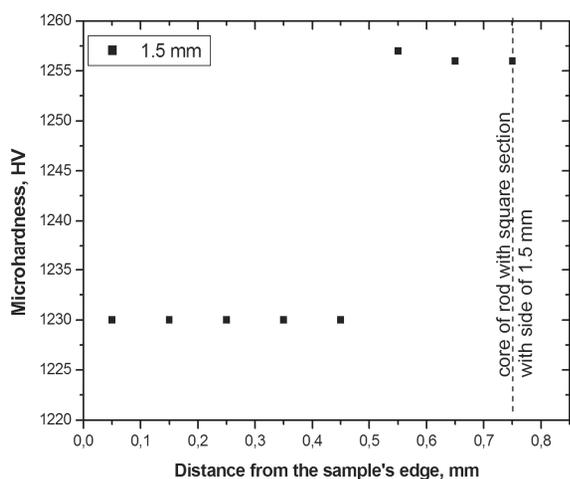
Fig. 19. Results of the microhardness experiments of $Fe_{36}Co_{36}B_{19}Si_5Nb_4$ rod with square section with side of 1.5 mm (cast 2) prepared from the industrial raw materials

- The rods with square section with side of 1.5 mm and 2.5 mm (cast 1) produced from high purity raw materials have amorphous structure.
- The thermal stability of the alloys prepared from high purity raw materials and from industrial materials are different. The base alloy's composition prepared from industrial raw materials is far away from the eutectic point, what results in the alloy's reduced glass forming ability.
- Microhardness of rods prepared from high purity raw materials insignificant changes in the function of the distance from the sample's edge as a result of relaxation process of structure.
- Microhardness of rods with square section with side of 1.5 and 2.5 mm (cast 1) prepared from the industrial raw materials are significantly different and dependent on type of phases existing in the structure. The microhardness of amorphous phase is far lower than that of crystalline phase occur in both alloys prepared with high cooling rate.

References

[1] A. Inoue, B.L. Shen, C.T. Chang, Fe- and Co-based bulk glossy alloys with ultrahigh strength of over 4000 MPa, Intermetallics 14 (2006) 936-944.

[2] M. Stoica, R. Li, A.R. Yavari, G. Vaughan, J. Eckert, N.V. Steenberge, D.R. Romera, Thermal stability and magnetic properties of FeCoBSiNb bulk metallic glasses, Journal of Alloys and Compounds 504S (2010) S123-S128.

[3] W. Pilarczyk, R. Nowosielski, R. Babilas, An attempt of selected metallic glasses producing with Fe and Ni matrix, Archives of Materials Science and Engineering 41/1 (2010) 5-12.

[4] R. Nowosielski, R. Babilas, Preparation, structure and properties of Fe-based bulk metallic glasses, Journal of Achievements in Materials and Manufacturing Engineering 40/2 (2010) 123-130.

[5] R. Nowosielski, R. Babilas, Glass-forming ability analysis of selected Fe-based bulk amorphous alloys, Journal of Achievements in Materials and Manufacturing Engineering 42 (2010) 66-72.

[6] R. Babilas, R. Nowosielski, Iron-based bulk amorphous alloys, Archives of Materials Science and Engineering 44/1 (2010) 5-27.

[7] S. Lesz, D. Szewieczek, J. Tyrlik-Held, Correlation between fracture morphology and mechanical properties of NANOPERM alloys, Archives of Materials Science and Engineering 29/2 (2008) 73-80.

[8] S. Lesz, S. Griner, R. Nowosielski, Influence of geometry of rapidly solidified rods on properties of Fe-Co-based alloy, Journal of Achievements in Materials and Manufacturing Engineering 41 (2010) 16-25.

[9] S. Lesz, Z. Stokłosa, R. Nowosielski: Influence of copper addition on properties of $(Fe_{36}Co_{36}B_{19}Si_5Nb_4)_{100-x}Cu_x$ metallic glasses, Archives of Materials Science and Engineering 38/1 (2009) 12-18.

[10] Z.H. Gan, H.Y. Yi, J. Pu, J.F.Wang, J.Z. Xiao, Preparation of bulk amorphous Fe-Ni-P-B-Ga alloys from industrial raw materials, Scripta Materialia 48 (2003) 1543-1547.

[11] H. Li, S. Yi, Fabrication of bulk metallic glasses in the alloy system Fe-C-Si-B-P-Cr-Mo-Al using hot metal and industrial ferro-alloys, Materials Science and Engineering A 449-451 (2007) 189-192.

[12] Y. Hu, M.X. Pan, L. Liu, Y.H. Zhao, D.Q. Zhao, W.H. Wang, Synthesis of Fe-based bulk metallic glasses with low purity materials by multi-metalloids addition, Materials Letters 57 (2003) 2698-2701.

[13] V. Ponnambalam, S.J. Poon, G.J. Shiflet, Fe-based bulk metallic glasses with diameter thickness larger than one centimeter, Journal of Materials Research 19/5 (2004) 1320-1323.

[14] Z.P. Lu, C.T. Liu, J.R. Thompson, W.D. Porter, Structural Amorphous Steels, Physical Review Letters 92/24 (2004) 245503-1- 245503-4.

[15] D.Y. Liu, W.S. Sun, H.F. Zhang, Z.Q. Hu, Preparation, thermal stability and magnetic properties of Fe-Co-Ni-Zr-Mo-B bulk metallic glass, Intermetallics 12 (2004) 1149- 1152.

[16] S.F. Guo, L. Liu, X. Lin, Formation of magnetic Fe-based bulk metallic glass under low vacuum, Journal of Alloys and Compounds 478 (2009) 226-228.

[17] W. Pilarczyk, R. Nowosielski, A. Januszka, Structure and properties of Fe-Cr-Mo-C bulk metallic glasses obtained by die casting method, Journal of Achievements in Materials and Manufacturing Engineering 42 (2010) 81-87.

[18] P. Kwapuliński, J. Rasek, Z. Stokłosa, G. Badura, B. Kostrubiec, G. Haneczok, Magnetic and mechanical properties in FeXSiB (X=Cu, Zr, Co) amorphous alloys, Archives of Materials Science and Engineering 31/1 (2008) 25-28.

[19] W.J. Boettinger, U.R. Kattner, K.-W. Moon, J.H. Perepezko, DTA and Heat flux DSC Measurements of Alloy Melting and Freezing, National Institute of Standards and Technology Special Publication 960-15 (2006).

[20] PN-EN ISO 6507-1:2007.

[21] J.T. Fan, Z.F. Zhang, S.X. Mao, B.L. Shen, A. Inoue, Deformation and fracture behaviors of Co-based metallic glass and its composite with dendrites, Intermetallics 17 (2009) 445-452.